Chapter 14
Molecular Simulation of Ionic Liquids: Complex Dynamics and Structure

Niki Vergadou

Abstract Ionic Liquids (ILs) are organic salts with melting temperatures below 100° C. They are characterized by an exceptional combination of properties that renders them very good candidates for use in many cutting-edge technological applications. The organic and simultaneously ionic nature of the constitutive ions results in diverse interactions that directly affect the microscopic structure and the dynamical behaviour of ILs. Molecular simulation methods using optimized force fields are applied for the study of the complex dynamics and the spatial organization in ILs.

14.1 Introduction to Ionic Liquids

Ionic fluids consist entirely of ions. Within this category of materials, a new class of fluids has emerged in the last few decades under the term "Ionic Liquids" (ILs) [1, 2]. ILs differ from molten salts due to the fact that they are usually composed of one large asymmetric cation and one organic or inorganic anion and the combination of this type of ionic chemical structures leads to salts with lower melting temperatures. Following the description of Paul Walden who was one of the first [3, 4] to observe organic salts in 1914, ILs are considered as the salts that are in the liquid state at room temperature and by convention below 100° C. In Fig. 14.1, some typical anions and cations are shown. There is a vast number of anions and cations that can be combined to form millions of potential ILs [5], revealing an enormous territory that despite having attracted great scientific interest in recent years, still remains largerly unexplored.

ILs are identified as novel designer solvents and advanced materials that can be utilized in a wide range of processes and applications. This fact is predominantly attributed to their great chemical tunability due to the diverse chemical structure of

N. Vergadou (✉)
Molecular Thermodynamics and Modelling of Materials Laboratory, Institute of Nanoscience and Nanotechnology, National Center for Scientific Research "Demokritos", 153 10 Aghia Paraskevi Attikis, Greece
e-mail: n.vergadou@inn.demokritos.gr

S. Lambropoulou et al. (eds.), *Algebraic Modeling of Topological and Computational Structures and Applications*, Springer Proceedings in Mathematics & Statistics 219, https://doi.org/10.1007/978-3-319-68103-0_14

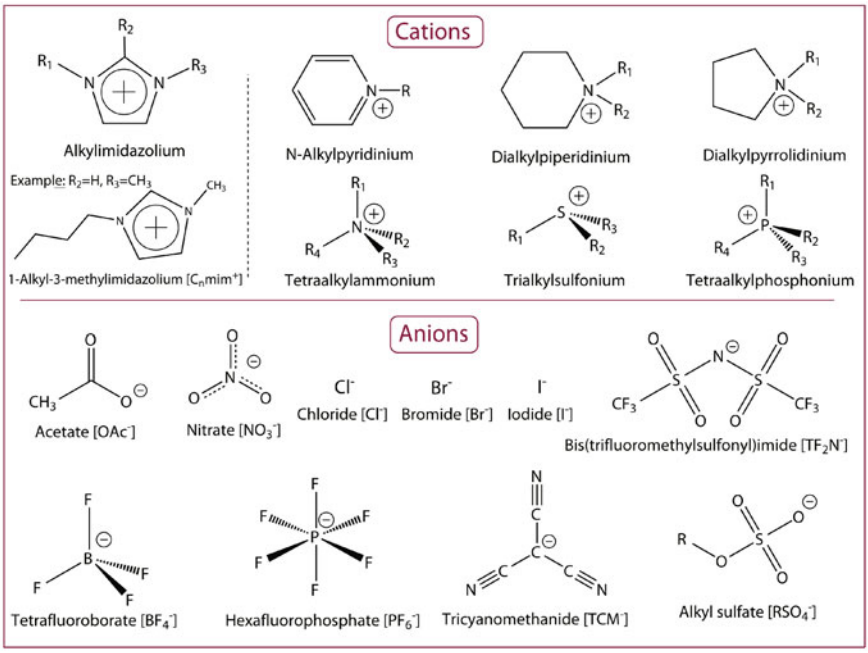

Fig. 14.1 Chemical structure of commonly used cations and anions

the anions and cations involved that enables the design of task specific ILs (TSILs) with controlled macroscopic properties. Apart from this important characteristic, ILs also combine a number of other exceptional properties [6–9] such as negligible vapour pressure, non-flammability, good thermal and electrochemical stability, wide range of temperatures over which they remain in the liquid state as well as very good solvation properties and in many cases high CO_2 absorption and separation capacity [10, 11]. Their range of application constantly grows and extends from green chemistry and electrochemistry to biotechnology, environmental engineering and novel separation processes (Fig. 14.2).

14.2 Molecular Simulation

The plethora of ILs and the multitude of technologies in which ILs can be used, necessitates the unraveling of the underlying mechanisms [12] that are responsible for their macroscopic behaviour. Molecular simulation [13, 14] is based on the fundamental principles of statistical mechanics and provides a unique systematic way in this direction, enabling at the same time the prediction of a number of materials properties. Among the properties that can be calculated from molecular simulations are: (i) ther-

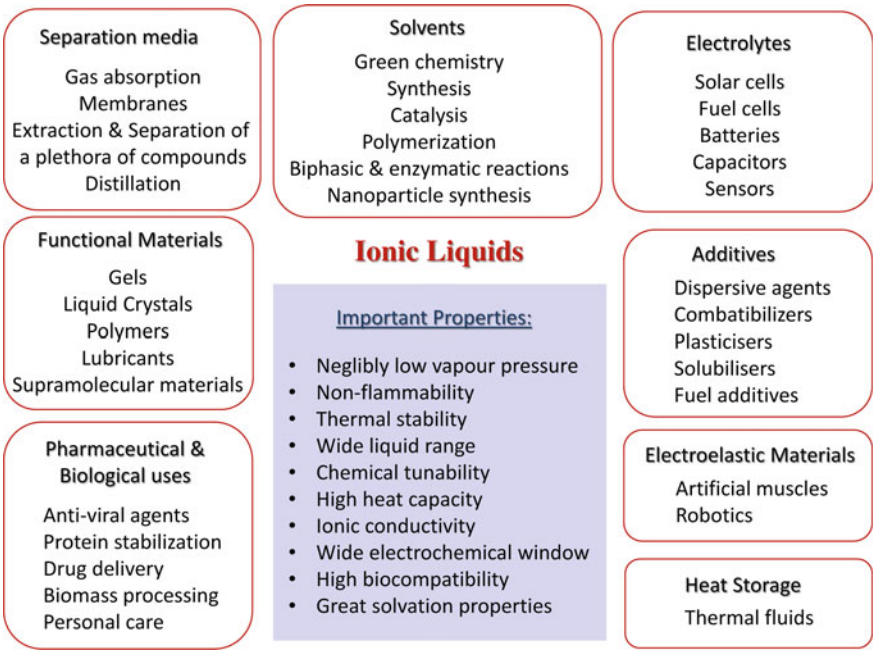

Fig. 14.2 Important properties of ILs and indicative range of applications

modynamic properties such as density, isothermal and isobaric compressibility, heat capacities, Gibbs free energy, Helmholtz free energy, activity coefficients, (ii) structural properties, (iii) dynamical and transport properties including local dynamics, diffusion coefficients, viscosities and ionic conductivities, (iv) surface and interfacial properties such as surface tension, (v) phase equilibria, (vi) mechanical properties and (vi) selectivity and permeability properties.

Various molecular simulation methods can be implemented depending on the materials under study and the time- and length-scales involved in the specific problem at hand, ranging from ab initio quantum mechanical methods, atomistic simulations (Monte Carlo, Molecular Dynamics, Transitions State Theory of Infrequent Events) to mesoscopic methods (Coarse-grained simulations, Kinetic Monte Carlo etc.). This chapter involves the computational study of ILs at the atomistic level using molecular dynamics (MD) simulation [15, 16].

The accuracy in the predictions of molecular simulation relies to a large extend on the force field used for the representation of the inter- and intramolecular interactions in the system. The interaction potential is typically of the form:

$$U = \sum_{bonds} k_b(l - l_0)^2 + \sum_{angles} k_\theta(\theta - \theta_0)^2 + \sum_{dihedrals} \sum_{n=1}^{4} k_\chi \left[1 + \cos\left(n\chi - \delta\right)\right] + \sum_{impropers} k_\psi \left(\psi - \psi_0\right)^2 + \sum_{\iota=1}^{n-1} \sum_{j>1}^{n} \left\{ 4\varepsilon_{ij} \left[\left(\frac{\sigma_{ij}}{r_{ij}}\right)^{12} - \left(\frac{\sigma_{ij}}{r_{ij}}\right)^{6} \right] + \frac{q_i q_i}{4\pi\varepsilon_0 r_{ij}} \right\} \tag{14.1}$$

where l, θ, χ and ψ denote bond length, bond angle, dihedral and improper angle, respectively, and the subscript "0" refers to the equilibrium values. In the dihedral potential term, parameter n is the multiplicity of the dihedral angle and δ is the phase shift of the dihedral potential over the full range of rotation. Partial charges are denoted by q_i, ε_0 is the vacuum permittivity and ε, σ are the Lennard-Jones (LJ) parameters.

There are several difficulties and challenges in the molecular simulation of ILs [17–19]. The intense chemical diversity that characterizes the ions in ILs, prohibits the use of general force fields and necessitates the development and optimization of system specific interaction potentials. At the same time, complex inter-ionic and strong electrostatic interactions are present in these systems, hence polarizability and charge transfer effects have to be taken into account in order to simulate accurately their behaviour.

14.3 IL Structure and Dynamics

ILs exhibit a wide range of time scales in the relaxation of their various modes of motion. They retain their structural organization at much longer distances compared to ordinary liquids and are characterized by a sluggish dynamical behavior. ILs are glass-forming materials and therefore the prediction of their transport properties, especially at low temperatures, is a very demanding task. The discussion that follows focuses on molecular simulation results on ILs with imidazolium-based cations, specifically the 1-alkyl-3-methylimidazolium ($[C_n mim^+]$) cations, varying the cations alkyl tail, coupled with bis(trifluoromethylsulfonyl)imide ($[TF_2N^-]$) or tricyanomethanide ($[TCM^-]$) anions. MD simulations of several tens of nanoseconds were performed in a wide temperature range, and at atmospheric pressure using classical force fields that have been optimized and extensively validated for these two imidazolium-based IL families [20, 21].

14.3.1 Spatial Organization

ILs are heterogeneous fluids that due to the ionic interactions, form polar and non-polar domains [22]. Structural order is retained at long distances and is clearly

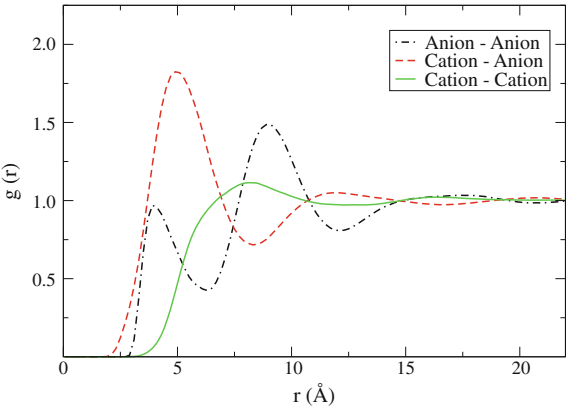

Fig. 14.3 Radial discribution functions (RDF) between the ions centers-of-mass of $[C_8mim^+][TCM^-]$ IL at 298 K [21]

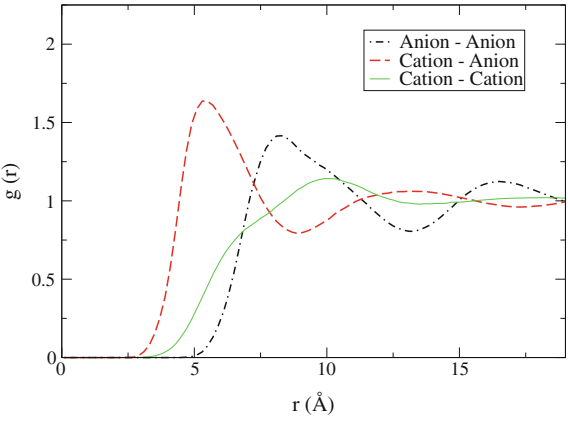

Fig. 14.4 Radial discribution functions (RDF) between the ions centers-of-mass of $[C_8mim^+][TF_2N^-]$ IL at 398 K [23]

depicted by intense oscillations in the radial distribution functions (RDF) [21, 23] of the ions center of mass. The anion-cation RDF reveals the strong ionic coupling of the counterions (Figs. 14.3 and 14.4) and exhibits multiple coordination shells (not in phase with the anion-anion RDF) while cation-cation RDFs show a much broader distribution. The spatial distribution function of the central carbon in $[TCM^-]$ around $[C_4mim^+]$ at 298K (using an iso-surface value equal to 8.1 nm^{-3}) is shown in Fig. 14.5.

The effect of the alkyl tail length on these properties was also investigated and tail aggregation phenomena (Fig. 14.6), which become more evident for the longer alkyl chain lengths, were detected by calculating radial distribution functions between different sites on the ions [20, 21, 23]. The microscopic local structure reflects a spatially heterogeneous environment that evolves from the interplay between short-range collective interactions (non-polar tail groups) and long-range electrostatic interactions (cation's head groups). For a larger number of carbon atoms in the cation's alkyl tail, liquid crystalline-like structures emerge [24].

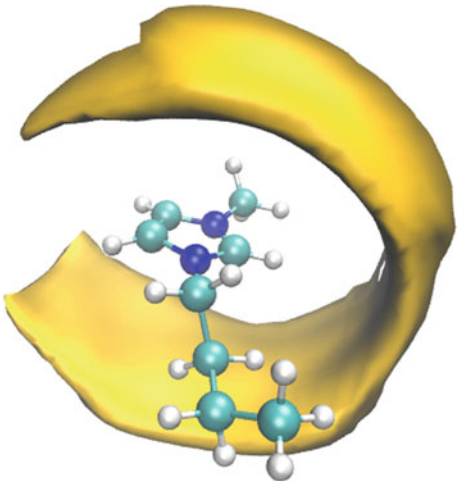

Fig. 14.5 Spatial distribution function of the central carbon in [TCM^-] around [C_4mim^+] (iso-surface value equal to 8.1 nm^{-3})

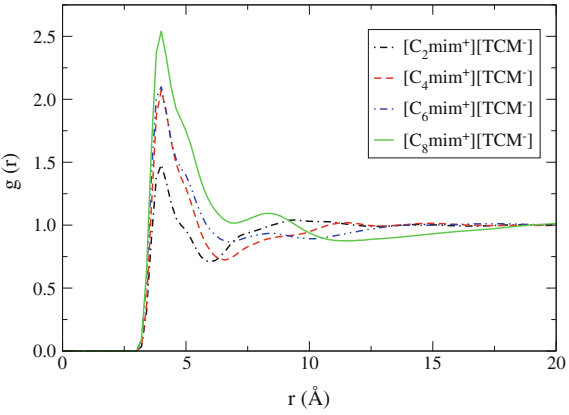

Fig. 14.6 Radial distribution function (RDF) between the terminal carbon atoms in the cation alkyl chain of [C_2mim^+][TCM^-] (black), [C_4mim^+][TCM^-] (red), [C_6mim^+][TCM^-] (blue) and [C_8mim^+][TCM^-] (green) at 298 K [21]

14.3.2 Dynamical Heterogeneity

ILs are viscous liquids and their dynamics often resembles the one of the supercooled liquids. Cooperative motion and caging effects are present in these systems leading to heterogeneity phenomena [25–30] and to a non-Arrhenius behaviour. In glass-forming materials, at short times the particles are trapped in "cages" of adjacent particles, while the escape from the cage takes place at longer time scales as the temperature decreases. Complex and heterogeneous dynamics has been detected in ILs both experimentally [31–35] and computationally [20, 21, 35–43]

An estimation of the time scales at which dynamic heterogeneity appears can be obtained from the non-Gaussian parameters $\alpha_n(t), n = 2, 3, \ldots$ [44], with $\alpha_2(t)$ defined as:

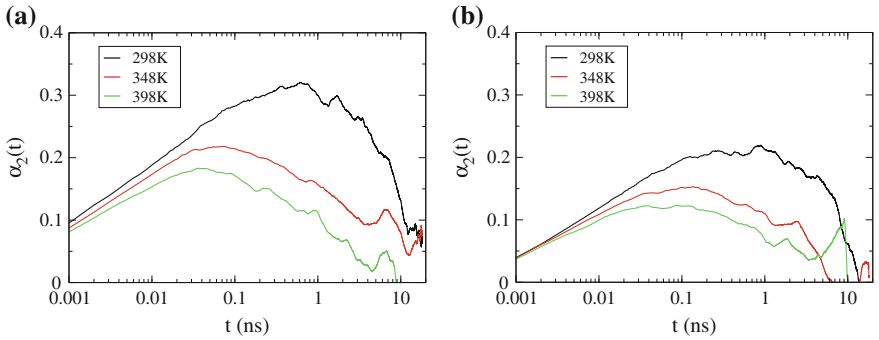

Fig. 14.7 Non-Gaussian parameter $\alpha_2(t)$ at 298, 348 and 398 K for **a** cation and **b** anion of $[C_8mim^+][TF_2N^-]$ IL [20]

$$\alpha_2(t) = \frac{3\langle|\mathbf{r}_i(t) - \mathbf{r}_i(t_0)|^4\rangle}{5\langle|\mathbf{r}_i(t) - \mathbf{r}_i(t_0)|^2\rangle^2} - 1 \tag{14.2}$$

where $|\mathbf{r}_i(t) - \mathbf{r}_i(t_0)|$ represents the displacement of a particle (or an ion's center of mass) at a time interval $t - t_0$ and the brackets denote the mean over all particles. Non-zero values in $\alpha_2(t)$ signify dynamical heterogeneity phenomena with the maximum being only indicative of the time of maximum heterogeneity, as the non-Gaussian behaviour may be preserved at much longer times [45, 46]. The ballistic motion is characterised by zero $\alpha_2(t)$ values and $\alpha_2(t)$ begins to increase at time scales associated with β relaxation, dropping again at the long time limit to zero (α relaxation) [47].

The non-Gaussian parameter is plotted in Fig. 14.7 for the cation and the anion in $[C_8mim^+][TF_2N^-]$ IL at three temperatures [20]. These plots clearly depict a non-Gaussian nature in both ions that is preserved at longer times, with the cation exhibiting a higher a_2 peak than the anion. This is also true for the ILs with the shorter alkyl tails [20] and is indicative of a more pronounced heterogeneous behaviour for the cation. The maxima obtain a higher value as the temperature decreases and at longer times. In case of $[C_nmim^+][TCM^-]$, the anion is the one with the more intense maximum [21, 48] as shown in Fig. 14.8 for $[C_8mim^+][TCM^-]$ cation and anion at 298 K.

A quantification of the dynamic heterogeneity can be achieved by measuring a time-space correlation function corresponding to a classical expression of van Hove function [49]:

$$G(\mathbf{r}, t) = \frac{1}{N}\left\langle \sum_{i=1}^{N}\sum_{j=1}^{N} \delta\left(\mathbf{r} - \mathbf{r}_i(t) + \mathbf{r}_j(0)\right)\right\rangle \tag{14.3}$$

where δ is Dirac delta and the brackets denote time average from an equilibrium trajectory in phase space. Therefore, although $G(\mathbf{r}, t)$ is a dynamic function, it is simultaneously a measure of an equilibrium property. The function $G(\mathbf{r}, t)$ is

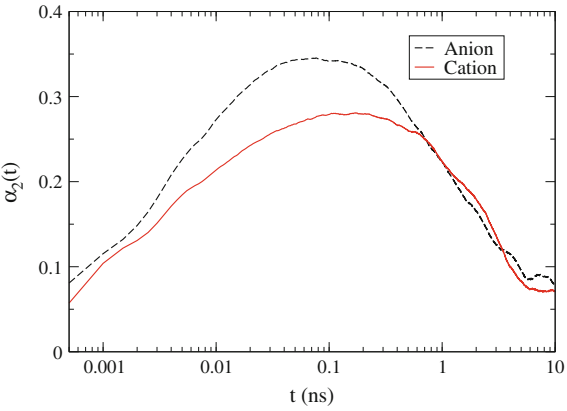

Fig. 14.8 Non-Gaussian parameter $\alpha_2(t)$ for the cation (red) and the anion (black) of [C_8mim^+] [TCM^-] IL at 298K [21]

proportional to the probability that a particle is located at position $\mathbf{r}$ at time t given that a particle was located at $\mathbf{r}(0)$ at $t = 0$ and can be separated in a self (G_s) for $i = j$ and a distinct part (G_d) for $i \neq j$:

$$G(\mathbf{r}, t) = G_s(\mathbf{r}, t) + G_d(\mathbf{r}, t) \tag{14.4}$$

Single-ion dynamics can be quantified by the self-part of the van Hove correlation function [50] that provides the distribution of particle dispacements for different times:

$$G_s(\mathbf{r}, t) = \frac{1}{N}\left\langle \sum_{i=1}^{N}\sum_{j=1}^{N} \delta(\mathbf{r} - \mathbf{r}_i(t) + \mathbf{r}_i(0)) \right\rangle \tag{14.5}$$

At time $t = 0$, $G_s(\mathbf{r}, 0) = \delta$ and for all times, it is normalized by:

$$\int G_s(\mathbf{r}, t)\, d\mathbf{r} = 1 \tag{14.6}$$

At the long time limit, the particle is independent of its initial position:

$$\lim_{r\to\infty} G_s(\mathbf{r}, t) = \lim_{t\to\infty} G_s(\mathbf{r}, t) = \frac{1}{V} \approx 0 \tag{14.7}$$

where V is the system volume. The probability density that a particle displaces by distance r [51] is given by:

$$g_s(r, t) = \int_{\theta=0}^{\pi}\int_{\phi=0}^{2\pi} G_s(\mathbf{r}, t)\, r^2 \sin\theta d\phi d\theta \tag{14.8}$$

and for an isotropic medium $G_s(\mathbf{r}, t) = G_s(r, t)$ and $g_s(r, t) = 4\pi r^2 G_s(r, t)$.

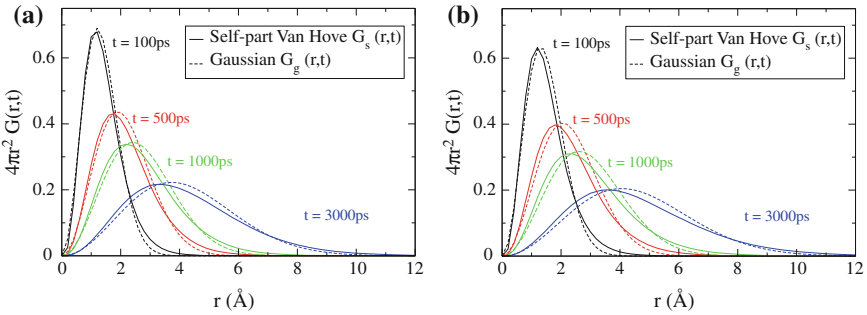

Fig. 14.9 Self-part of the Van Hove function $G_s\,(r, t)$ as a function of distance at 298 K plotted against the expected Gaussian distribution for **a** the cation and **b** the anion of $[C_6mim^+][TCM^-]$

In the case of Fickian diffusion, the self-part of the Van Hove function follows the Gaussian approximation [52]:

$$G_s{}^g\,(r, t) = \left[\frac{3}{2\pi\left\langle \Delta r^2(t)\right\rangle}\right]^{\frac{3}{2}} \exp\left[\frac{-3r^2}{2\left\langle \Delta r^2(t)\right\rangle}\right] \tag{14.9}$$

with $\left\langle \Delta r^2(t)\right\rangle$ being the mean square displacement (MSD) at a time interval t.

In Fig. 14.9, the self-part of the Van Hove function $G_s\,(r, t)$ for (a) the cation and (b) the anion of $[C_6mim^+][TCM^-]$ [21] is plotted against the expected Gaussian distribution at 298 K and for t = 100, 500, 1000, 3000 ps. Deviations of the $G_s\,(r, t)$ from the expected Gaussian are evidence of dynamic heterogeneity, which for the systems under study is present at time intervals typically ranging from a few ps up to several ns. For the longer alkyl tail IL, the non-Gaussian behavior persists at longer times, while these deviations are diminished as the temperature is increased. A multifractal character has been also reported [42] in relation to the heterogeneous nature of ILs.

The divergence between the $G_s\,(r, t)$ and $G_s{}^g\,(r, t)$ curves depicts the existence at intermediate times of ions with "faster" or "slower" mobility than expected based on that distance that each ion has travelled at time t. The crossing points of the two curves at short and long distances are used to identify dynamically distinguishable ions at a specific time interval [47].

The spatial correlation of these subsets of fast and slow ions manifests the occurrence of clustering phenomena between mobile and immobile ions. This is clearly shown in Fig. 14.10, in which the RDFs between the centers of mass of slow anions – slow cations, fast anions – fast cations and fast – slow anions and cations are shown for (a) $[C_4mim^+][TCM^-]$ [21] and (b) $[C_6mim^+][TCM^-]$ at 298 K for t = 500 ps. These RDFs are plotted against the RDF that corresponds to the anion-cation centers of mass as calculated from all ions, exhibiting maxima at the same distances with much higher peaks, though, in the case of ions of same mobility. The evolution of

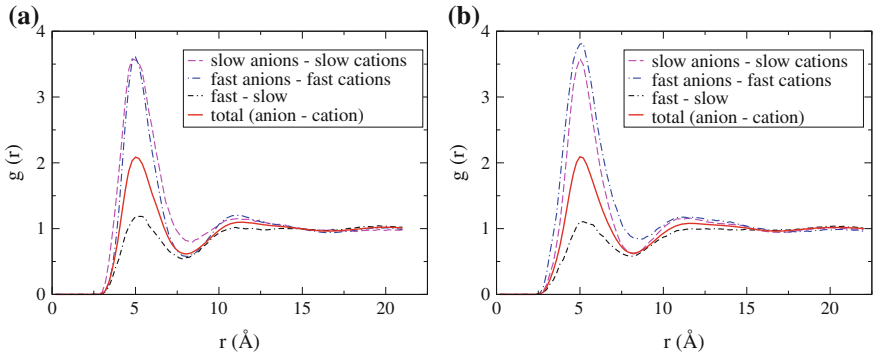

Fig. 14.10 Radial distribution functions (RDF) between the centers of mass of slow anions slow cations (magenta), fast anions fast cations (blue) and fast slow anions and cations (black) plotted against the total RDF (red) calculated for **a** $[C_6mim^+][TCM^-]$ [21] and **b** $[C_6mim^+][TCM^-]$ at 298 K for t = 500 ps. The red line corresponds to the radial distribution functions between the anion-cation centers of mass as calculated from all ions

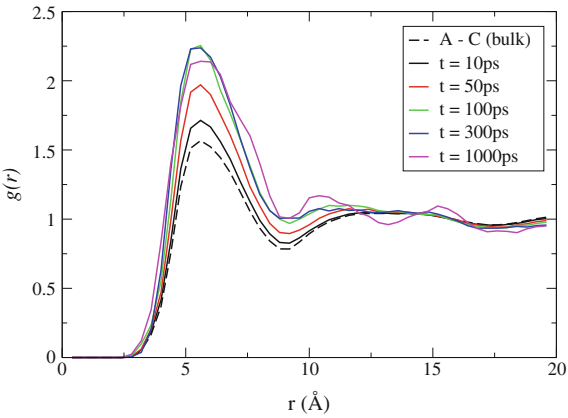

Fig. 14.11 Radial distribution functions between the centers of mass of fast cations and fast anions calculated at 298 K for t = 10, 50, 100, 300 and 1000 ps of $[C_8mim^+][TF_2N^-]$ [20]

the clustering tendency in time is shown in Fig. 14.11 as calculated for fast cations and fast anions of $[C_8mim^+][TF_2N^-]$ at 298 K and t = 10, 50, 100, 300 and 1000 ps [20].

14.3.3 Diffusional Anisotropy

Anisotropy in the ions translational motion is present in some ionic species in ILs [20, 21, 40, 53]. Such phenomena can be traced by examining the ions diffusional motion along specific axes dictated by the geometry of the ions. In Fig. 14.12, four axes are defined for the case of imidazolium-based cations: the vector NN that connects the

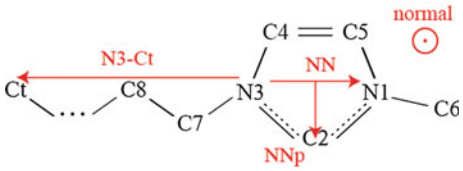

Fig. 14.12 The vectors defined on the imidazolium-based cation along which the translational motion of the center of mass was analyzed

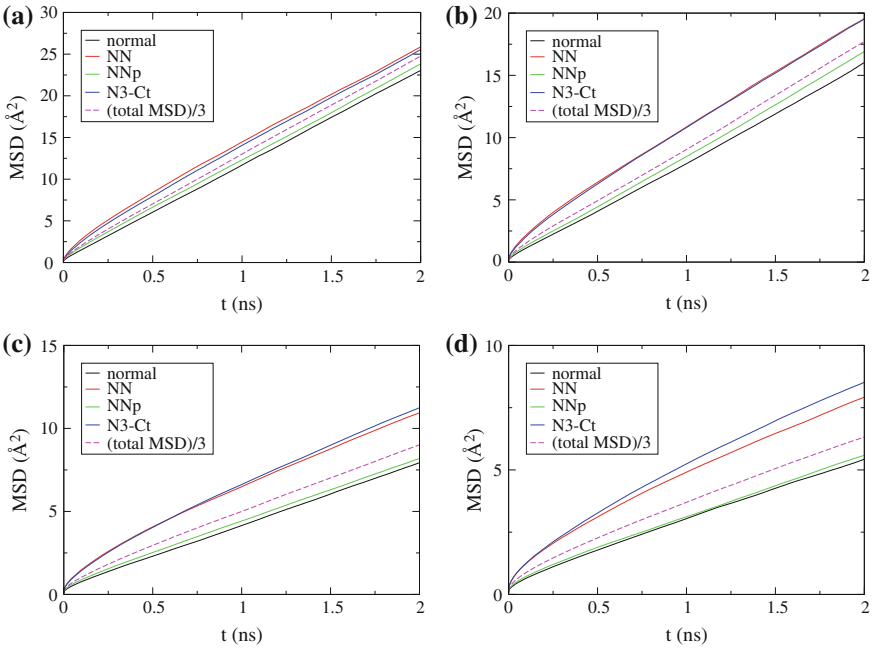

Fig. 14.13 Mean square displacement (MSD) at 298 K calculated along the direction of the vector that is normal to the imidazolium plane (black), the vectors NN (red) and NNp (green), and along the the end-to-end vector N3-Ct of the alkyl tail (blue) of the cation compared to the 1/3 of the total MSD of the center of mass (magenta dashed line) for **a** [C_2mim$^+$][TCM$^-$], **b** [C_4mim$^+$][TCM$^-$], **c** [C_6mim$^+$][TCM$^-$] and **d** [C_8mim$^+$][TCM$^-$] [21]

two nitrogen atoms in the imidazolium ring, the normal vector to the imidazolium ring, the vector NNp that is perpendicular to the former two vectors and the end-to-end vector N3-Ct of the alkyl tail.

Diffusional anisotropy can be extracted by comparing the MSD along each axis to the one third of the total MSD, as shown in Fig. 14.13 for the cations in [C_2mim$^+$][TCM$^-$], [C_4mim$^+$][TCM$^-$], [C_6mim$^+$][TCM$^-$] and [C_8mim$^+$][TCM$^-$] ILs at 298K. In case of an isotropic diffusional motion the MSD along any axis would coincide with the total MSD/3. For all systems presented, there is a more facile movement along the NN and N3-Ct vectors, which becomes more intense for

the cations with the longer alkyl tails. For $[C_8mim^+][TCM^-]$ IL in particular, the movement along the N3-Ct vector deviates from the one of NN vector, exhibiting at 1.5ns an MSD almost by a factor of two higher than the 1/3 of the total MSD. The movement along the NNp vector and the vector that is normal to the imidazolium plane appears to be rather hindered compared to the other two directions. At 298K, diffusional anisotropy is maintained over long timescales that extend even to the Einstein regime. Similar behaviour is observed for the $[C_nmim^+][TF_2N^-]$ ILs in which, apart from the cation, there is also a preferential movement along the direction of the vector that connects the two sulfurs of the $[TF_2N^-]$ anion [20].

14.3.4 Transport Properties

Long MD simulations in the order of several tens of nanoseconds have been performed for the determination of the transport properties of the ILs under study. The self-diffusion coefficients of the ions were calculated using the Einstein relation [54]:

$$D = \frac{1}{2d} \lim_{t\to\infty} \frac{d}{dt} \left\langle |\mathbf{r}_i(t) - \mathbf{r}_i(0)|^2 \right\rangle \tag{14.10}$$

where the brackets indicate the mean square displacement (MSD) over all ions' centers of mass and d is the dimensionality of the conducted diffusivity.

The determination of the diffusion coefficients from an MD simulation presupposes that the system is simulated long enough, so that it has reached the Fickian regime. Normal diffusivity can be identified by a slope equal to unity in the log(MSD) versus log(t) plot. Self-diffusion coefficients were calculated for imidazolium-based ILs under study [20, 21, 48]. The self-diffusion coefficients for the ions in $[C_8mim^+][TCM^-]$ IL are shown in Fig. 14.14 at various temperatures and at atmospheric pressure. The calculated diffusivities for the cation are in excel-

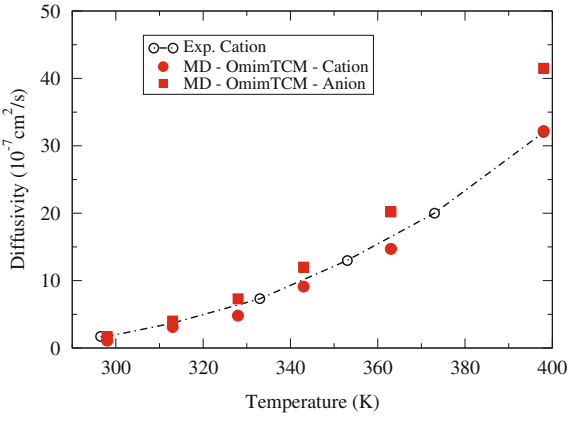

Fig. 14.14 Self-diffusion coefficients [21, 48] of the anion (*squares*) and the cation (*circles*) versus temperature for $[C_8mim^+][TCM^-]$ IL. The open points correspond to NMR experimental measurements for the cation [55]

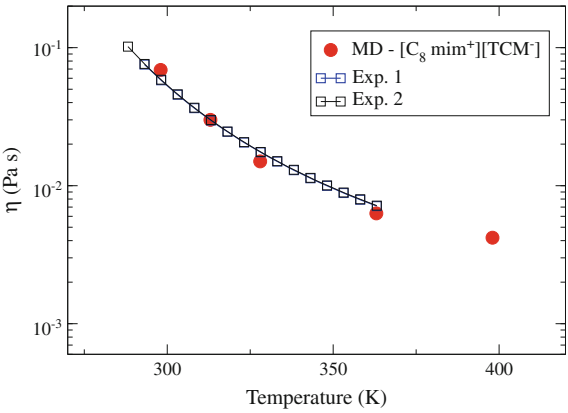

Fig. 14.15 Viscosity calculations from MD simulations (full points) [21, 48] as a function of temperature plotted against experimental data (lines with open points) [48, 56] for $[C_8mim^+][TCM^-]$

lent agreement with NMR experimental measurements [55] of the same IL system, confirming the ability of the recently optimized force field [21] to reproduce the properties of the $[C_nmim^+][TCM^-]$ IL family with great accuracy. No experimental results are currently available for the $[TCM^-]$ anion.

Shear viscosity was extracted from the autocorrelation function of the pressure tensor using the Green-Kubo relation:

$$\eta = \frac{V}{k_B T} \int_0^\infty dt \left\langle P_{\alpha\beta}(t) P_{\alpha\beta}(0) \right\rangle \tag{14.11}$$

where $P_{\alpha\beta}(t)$ is the $\alpha\beta$-element of the pressure tensor at time t ($\alpha \neq \beta$). The temperature dependence of the viscosity is captured very well [20, 21, 48] for all ILs with good agreement with available experimental data. In Fig. 14.15, viscosities calculated from MD in a wide temperature range for $[C_8mim^+][TCM^-]$ are plotted against experimental measurements exhibiting a very good agreement.

14.4 Conclusions

Ionic fluids inherently carry a higher degree of complexity than systems comprised of neutral species. ILs, in particular, exhibit an exceptional combination of properties that originate significantly from their dual organic and ionic nature. A fundamental understanding of the diverse interactions and the microscopic mechanisms that give rise to the non-trivial spatial and dynamical behaviour in ILs is required, especially considering more complex IL systems such as multi-compound IL fluids, ILs as gas separation media [10, 57] and under confinement in solid substrates [58, 59] or IL-IL mixtures [60, 61]. Theoretical and computational studies combined in a synergistic manner with high-resolution experimental techniques should target in elucidating the underlying complex phenomena, extending the fundamental knowledge and reveal-

ing the chemical structure – property relations in this class of advanced materials with enormous applicability in a wide range of state-of-the art technologies.

References

1. Holbrey, J., Seddon, K.: Ionic liquids. Clean Prod. Process. **1**, 223–236 (1999)
2. Wasserscheid, P., Welton, T.: Ionic Liquids in Synthesis, 2nd edn. Wiley-VCH Weinheim, Germany (2008)
3. Gabriel, S., Weiner, J.: Ueber einige Abkömmlinge des Propylamins. Ber. Dtsch. Chem. Ges. **21**, 2669–2679 (1888)
4. Walden, P.: Ueber die Molekulargrösse und elektrische Leitfähigkeit einiger geschmolzener Salze. Bull. Acad. Imp. Sci. (St. Ptersbourg) **8**, 405–422 (1914)
5. Rogers, R.D.: Reflections on ionic liquids. Nature **447**, 917–918 (2007)
6. Kirchner, B. (ed.): Topics in Current Chemistry- Ionic Liquids, vol. 290. Springer, Berlin (2010)
7. Handy, S.T. (ed.): Ionic Liquids - Classes and Properties. InTech, Rijeka, Croatia (2011)
8. Zhang, S., Lu, X., Zhou, Q., Li, X., Zhang, X., Li, S.: Ionic Liquids - Physicochemical Properties. Elsevier, Amsterdam (2009)
9. Visser, A.E., Bridges, N.J., Rogers, R.D. (eds.): Ionic Liquids: Science and Applications. ACS Symposium Series, vol. 1117 (2012)
10. Vergadou, N., Androulaki, E., Economou, I.G.: Molecular simulation methods for CO_2 capture and gas separation with emphasis on ionic liquids. In: Papadopoulos, A.I., Seferlis, P. (eds.) Process Systems and Materials for CO2 Capture: Modelling, Design, Control and Integration, pp. 79–111. Wiley, Chichester (2017)
11. Radmin, M., de Loos, T.W., Vlugt, T.J.H.: State-of-the-Art of CO2 capture with ionic liquids. Ind. Eng. Chem. Res. **51**, 8149–8177 (2012)
12. Weingärtner, H.: Understanding ionic liquids at the molecular level: facts, problems, and controversies. Angew. Chem. - Int. Edition **47**(4), 654–670 (2008)
13. Allen, M.P., Tildesley, D.J.: Computer Simulation of Liquids. Oxford University Press, Oxford (1987)
14. Frenkel, D., Smit, B.: Understanding Molecular Simulation - From Algorithms to Applications. Academic Press, San Diego (2002)
15. Haile, J.M.: Molecular Dynamics Simulation: Elementary Methods. Wiley, New York (1992)
16. Rapaport, D.C.: The Art of Molecular Dynamics Simulation, 2nd edn. Cambridge University Press, Cambridge (2004)
17. Salanne, M.: Simulations of room temperature ionic liquids: from polarizable to coarse-grained force fields. Phys. Chem. Chem. Phys. **17**, 14270–14279 (2015)
18. Batista, M.L.S., Coutinho, J.A.P., Gomes, J.R.B.: Prediction of ionic liquids properties through molecular dynamics simulations. Curr. Phys. Chem. **4**, 151–172 (2014)
19. Dommert, F., Wendler, K., Berger, R., Delle Site, L., Holm, C.: Force fields for studying the structure and dynamics of ionic liquids: a critical review of recent developments. Chem. Phys. Chem. **13**(7), 1625–1637 (2012)
20. Androulaki, E., Vergadou, N., Economou, I.G.: Analysis of the heterogeneous dynamics of imidazolium-based [Tf_2N^-] ionic liquids using molecular simulation. Mol. Phys. **112**, 2694–2706 (2014)
21. Vergadou, N., Androulaki, E., Hill, J.-R., Economou, I.G.: Molecular simulations of imidazolium-based tricyanomethanide ionic liquids using an optimized classical force field. Phys. Chem. Chem. Phys. **18**, 6850–6860 (2016)
22. Wang, Y., Voth, G.A.: Unique spatial heterogeneity in ionic liquids. J. Am. Chem. Soc. **127**, 12192–12193 (2005)
23. Androulaki, E., Vergadou, N., Ramos, J., Economou, I.G.: Structure, thermodynamic and transport properties of imidazolium-based bis(trifluoromethylsulfonyl)imide ionic liquids from molecular dynamics simulations. Mol. Phys. **110**(11–12), 1139–1152 (2012)

24. Ji, Y., Shi, R., Wang, Y., Saielli, G.: Effect of the chain length on the structure of ionic liquids: from spatial heterogeneity to ionic liquid crystals. J. Phys. Chem. B **117**, 1104–1109 (2013)
25. Donati, C., Glotzer, S.C., Poole, P.H., Kob, W., Plimpton, S.J.: Spatial correlations of mobility and immobility in a glass-forming Lennard-Jones liquid. Phys. Rev. E **60**(3), 3107–3119 (1999)
26. Qian, J., Hentschke, R., Heuer, A.: On the origin of dynamic heterogeneities in glass-forming liquids. J. Chem. Phys. **111**(22), 10177–10182 (1999)
27. Ediger, M.D.: Spatially heterogeneous dynamics in supercooled liquids. Annu. Rev. Phys. Chem. **51**, 99–128 (2000)
28. Debenedetti, P.G., Stillinger, F.H.: Supercooled liquids and the glass transition. Nature **410**, 259–267 (2001)
29. Richert, R.: Heterogeneous dynamics in liquids: fluctuations in space and time. J. Phys.: Condens. Matter **14**(23), R703–R738 (2002)
30. Chaudhuri, P., Sastry, S., Kob, W.: Tracking heterogeneous dynamics during the alpha relaxation of a simple glass former. Phys. Rev. Lett. **101**(19), 190601 (2008)
31. Paul, A., Mandal, P.K., Samanta, A.: On the optical properties of the imidazolium ionic liquids. J. Phys. Chem. B **109**(18), 9148–9153 (2005)
32. Aki, S.N.V.K., Brennecke, J.F., Samanta, A.: How polar are room-temperature ionic liquids? Chem. Commun. **5**, 413–414 (2001)
33. Ito, N., Arzhantsev, S., Maroncelli, M.: The probe dependence of solvation dynamics and rotation in the ionic liquid 1-butyl-3-methyl-imidazolium hexafluorophosphate. Chem. Phys. Lett. **396**(1–3), 83–91 (2004)
34. Jin, H., Li, X., Maroncelli, M.: Heterogeneous solute dynamics in room temperature ionic liquids. J. Phys. Chem. B **111**(48), 13473–13478 (2007)
35. Hu, Z., Margulis, C.J.: Heterogeneity in a room-temperature ionic liquid: persistent local environments and the red-edge effect. Proc. Nat. Acad. Sci. USA **103**(4), 831–836 (2006)
36. Del Pópolo, M.G., Voth, G.A.: On the structure and dynamics of ionic liquids. J. Phys. Chem. B **108**(5), 1744–1752 (2004)
37. Ishida, T., Shirota, H.: Dicationic versus monocationic ionic liquids: distinctive ionic dynamics and dynamical heterogeneity. J. Phys. Chem. B **117**(4), 1136–1150 (2013)
38. Habasaki, J., Ngai, K.L.: Molecular dynamics studies of ionically conducting glasses and ionic liquids: wave number dependence of intermediate scattering function. J. Chem. Phys. **133**(12), 124505 (2010)
39. Urahata, S.M., Ribeiro, M.C.C.: Unraveling dynamical heterogeneity in the ionic liquid 1-Butyl-3-methylimidazolium chloride. J. Phys. Chem. Lett. **1**(11), 1738–1742 (2010)
40. Liu, H., Maginn, E.: A molecular dynamics investigation of the structural and dynamic properties of the ionic liquid 1-n-butyl-3-methylimidazolium bis(trifluoromethanesulfonyl)imide. J. Chem. Phys. **135**(12), 124507 (2011)
41. Hu, Z., Margulis, C.J.: Room-temperature ionic liquids: slow dynamics, viscosity and the red edge effect. Acc. Chem. Res. **40**(11), 1097–1105 (2007)
42. Habasaki, J., Ngai, K.L.: Multifractal nature of heterogeneous dynamics and structures in glass forming ionic liquids. J. Non-Cryst. Solids **357**(2), 446–453 (2011)
43. Jeong, D., Choi, M.Y., Kim, H.J., Jung, Y.: Fragility, Stokes-Einstein violation, and correlated local excitations in a coarse-grained model of an ionic liquid. Phys. Chem. Chem. Phys. **12**, 2001–2010 (2010)
44. Rahman, A.: Correlations in the motion of atoms in liquid argon. Phys. Rev. **136**(2A), A405–A411 (1964)
45. Szamel, G., Flenner, E.: Independence of the relaxation of a supercooled fluid from its microscopic dynamics: Need for yet another extension of the mode-coupling theory. Europhys. Lett. **67**, 779–785 (2004)
46. Reichman, D.R., Rabani, E., Geissler, P.L.: Comparison of dynamical heterogeneity in hard-sphere and attractive glass formers. J. Phys. Chem. B **109**, 14654–14658 (2005)
47. Kob, W., Donati, C., Plimpton, S.J., Poole, P.H., Glotzer, S.C.: Dynamical heterogeneities in a supercooled Lennard-Jones liquid. Phys. Rev. Lett. **79**(15), 2827–2830 (1997)

48. Zubeir, L.F., Rocha, M.A.A., Vergadou, N., Weggemans, W.M.A., Peristeras, L.D., Schulz, P.S., Economou, I.G., Kroon, M.C.: Thermophysical properties of imidazolium tricyanomethanide ionic liquids: experiments and molecular simulation. Phys. Chem. Chem. Phys. **18**, 23121–23138 (2016)
49. Van Hove, L.: Correlations in space and time and born approximation scattering in systems of interacting particles. Phys. Rev. **95**(1), 249–262 (1954)
50. Berne, B.J., Harp, G.D.: On the calculation of time correlation functions. In: Prigogine, I., Rice, S.A. (eds.) Advances in Chemical Physics, vol. XVII, pp. 63–227. Wiley, Honoken (1970)
51. Gaub, M., Fritzsche, S., Haberlandt, R., Theodorou, D.N.: Van Hove function for diffusion in zeolites. J. Phys. Chem. B **103**(22), 4721–4729 (1999)
52. Vineyard, G.H.: Scattering of slow neutrons by a liquid. Phys. Rev. **110**(5), 999–1010 (1958)
53. Urahata, S.M., Ribeiro, M.C.: Single particle dynamics in ionic liquids of 1-alkyl-3-methylimidazolium cations. J. Chem. Phys. **122**(2), 024511 (2005)
54. Einstein, A.: Investigations on the Theory of the Brownian Movement. Dover, New York (1956)
55. Papavassiliou, G., Fardis, M.: Nuclear Magnetic Resonance Laboratory, Institute of Nanoscience and Nanotechnology, NCSR "Demokritos", Greece - Unpublished results
56. Romanos, G.E., Zubeir, L.F., Likodimos, V., Falaras, P., Kroon, M.C., Iliev, B., Adamova, G., Schubert, T.J.S.: Enhanced CO2 capture in binary mixtures of 1-alkyl-3-methylimidazolium tricyanomethanide ionic liquids with water. J. Phys. Chem. B **117**, 12234–12251 (2013)
57. Bara, J.E.: Ionic liquids in gas separation membranes. In: Hoek, E.M.V., Tarabara, V.V. (eds.) Encyclopedia of Membrane Science and Technology, pp. 1–23. Wiley, Hoboken (2013)
58. Kritikos, G., Vergadou, N., Economou, I.G.: Molecular dynamics simulation of highly confined glassy ionic liquids. J. Phys. Chem. C **120**(2), 1013–1024 (2016)
59. Sha, M., Dou, Q., Wu, G.: Molecular dynamics simulation of ionic liquids adsorbed onto a solid surface and confined in nanospace. In: Springborg, M. (ed.) Chemical Modelling: Applications and Theory, vol. 9, pp. 186–217. The Royal Society of Chemistry, Cambridge (2012)
60. Chatel, G., Pereira, J.F.B., Debbeti, V., Wang, H., Rogers, R.D.: Mixing ionic liquids - "simple mixtures" or "double salts"? Green Chem. **16**(4), 2051–2083 (2014)
61. Niedermeyer, H., Hallett, J.P., Villar-Garcia, I.J., Hunt, P.A., Welton, T.: Mixtures of ionic liquids. Chem. Soc. Rev. **41**(23), 7780–7802 (2012)